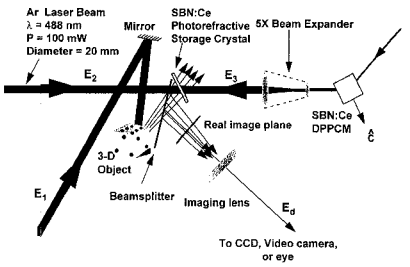

CTuP10 Fig. 1 Experimental setup used to record and display/observe hologram(s).

introduced into a Ce-doped SBN:60 double-pumped phase-conjugate mirror to produce the phase conjugate of the reference beam that then acts as the read beam (E_3). Use of the phase conjugate as the read beam guarantees that all field angles of the hologram are accurately reproduced via their gratings' respective Bragg angles.[1] A beamsplitter placed between the object and crystal enables separate viewing/displaying of the real hologram. Direct observation of the projected 3-D hologram via the eye or video camera indicates that the observed field of view (OFOV) is limited to approximately 5°, a value that is less than the maximum geometrically limited field-of-view (GFOV) estimated to be approximately 15°. The latter may be understood as follows: If the crystal is assumed to be a window with the observer looking through this window at the object, then the GFOV is the range of angles over which the object can be observed before the edges of the window begin to eclipse the object. Since the hologram is an exact replication of the object, the OFOV is limited to the GFOV.

Our approach to increase the limited OFOV is to image the hologram into a suitable scattering medium to facilitate observation over the entire GFOV. The ability to distinguish separate views of the hologram will be an important test of the performance of such a medium. Results to date indicate that when the 3-D image is projected into a scattering medium it is possible to observe and record the image at an OFOV comparable to the maximum GFOV. The resolution limits, optimum particle density, maximum GFOV, as well as other pertinent parameters related to this display technique are being investigated and will be discussed.

1. R. J. Anderson, B. P. Ketchel, G. L. Wood, G. J. Salamo, paper NThA4-1, Nonlinear Optics: Materials, Fundamentals, and Applications, Maui, Haw. (1996).
2. J. Ma, T. Chang, J. Hong, R. R. Neurgonkar, G. Barbastathis, D. Psaltis, paper JTuB4-1, Nonlinear Optics: Materials, Fundamentals, and Applications, Maui, Haw. (1996).

CTuP11

Resonant photoexcitation modes in azo dye-doped nematics

T. V. Galstyan, B. Saad, M. M. Denariez-Roberge, *Université Laval, Centre d'Optique, Photonique et Laser, Québec, Canada; E-mail: galstian@phy.ulaval.ca*

Dye-doped liquid crystal (LC) materials actually attract very intensive studies in view of their application in optical addressing systems. In this work, we investigate the photoisomerization of two azobenzene dichroic dyes and the excitation transfer from the dye to the nematic liquid crystal (NLC) host. These dyes contain one and two azo bonds and are named by us, D1 and D2 (by Merck's notation), respectively. We use the dynamic diffraction and polarization techniques for this study. The host for both dyes is a homeotropically oriented 4,4′-cyanoamylbiphenyl NLC cell. The guest-host system is prepared by dye volume doping in 1 Wt % concentration. The use of CW laser step-like radiation allows us the study of both transient and stabilized regimes of interaction and identification of several scalar and anisotropy excitation mechanisms. The photoexcitation process is studied also for different wavelengths and intensities.

Strongly amplified rotation of nematic molecules is observed that depends dramatically on the photoexcitation wavelength. This amplification, e.g., for the D2 dye, is more efficient (by a factor 10) for the excitation wavelength in the red rather than the blue side of its absorption band. Transient periodic modulation of the nematic order parameter, three- and two-dimensional molecular transient rotation, and equilibrated two-dimensional molecular periodic rotation are observed and studied.

The obtained excitation modes are different for D1 and D2 dye-doped systems (Fig. 1). Thus certain transient excitation modes of D2 doped system (D2/NLC) are absent or strongly suppressed in D1 doped system (D1/NLC), while others are significantly changed in the character. For example, the intensity dependence in D1/NLC system reveals the presence of new transient excitation mode that has a stable saturation level, in contrast to the case of D2/NLC system. Long scale three-dimensional molecular rotations detected in D2/NLC are strongly suppressed in D1/NLC, etc.

The comparison of molecular structures of two azo dyes and observed differences in induced anisotropy and dynamic diffraction experiments provide interesting information about the presence of different excitation modes in each dye molecule himself and the possible modes of the excitation transfer to the host. These results are important for the better understanding of photoexcited dye induced dichroic torque, corresponding rotation of LC molecules and its applications in optical addressing systems.

We present the experimental setup, corresponding conditions, and principal experimental results. The nature of observed phenomena, in particular, their dependence upon the excitation wavelength and intensity are discussed. The possible role of the photoisomerization mechanism in observed excitation modes is detailed. In particular, the presence of long living intermediate states during dyes photoisomerization is suggested.

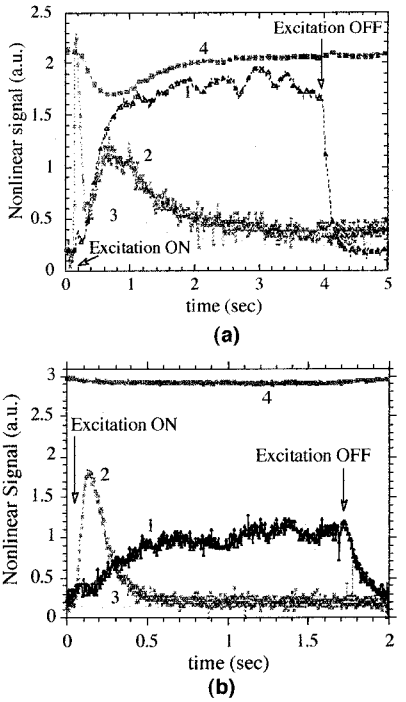

CTuP11 Fig. 1 Qualitative demonstration of the typical dynamic behavior of the excitation in azo dye-doped NLC. The excitation beams (the wavelength is 514 nm) have horizontal polarization, in the same plane as the director of NLC. Lines are used for better visibility only. Two curves 1 and 2 correspond to the diffraction signals for input polarization of the probe beam, parallel and perpendicular to the horizontal plane, respectively. They indicate the scalar or vector character of the excitation, for example, the two- and three-dimensional molecular rotations. Curves 3 and 4 represent the directly transmitted through the cell probe beam detected after the crossed and parallel analyzer orientation, respectively. This signals indicates the three-dimensional molecular rotation. (a) for the D2 dye-doped system. Mutual scale calibration of curves would require the following multiplication of scales: for the curves 1 and 3 by a factor 5, curves 2 and 4 by 10. (b) for the D1 dye-doped system in the same experimental conditions.

CTuP 12

Special angle cut of potassium niobate crystal for thermal fixing

Xiaolin Tong, Amnon Yariv, Aharon Agranat,* *California Institute of Technology, Pasadena, California 91125; E-mail: xltong@cco.caltech.edu*

We investigated the optimal cut of potassium niobate crystals to approach the maximum exponential photorefractive gain coefficient and the highest diffraction efficiency. Volume hologram is thermally fixed in this sample and a significant enhancement of diffraction efficiency is achieved.

The value of the exponential gain coefficient Γ depends both on the material parame-

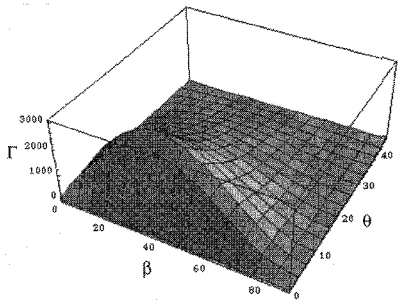

CTuP12 Fig. 1 Computer-generated three-dimensional plot of the exponential gain coefficient Γ versus the angle β and θ. Roughly speaking, the maximum Γ is corresponding to β = 40° and θ = 8°. Γ unit is m^{-1}.

ters (such as the density of mobile charges N_A, the electro-optic coefficient r_{ij}, and the dielectric constant ε) as well as external controlled parameters (such as the angle 2θ between the two beams, and the angle β between the grating vector and the *c* axis of the crystal). Assuming that the induced index grating is phase shifted by π/2 relative to the intensity distribution, the exponential gain coefficient Γ is

$$\Gamma = \frac{\omega}{2nc}\frac{E_{sc}\gamma_{\text{eff}}}{\cos\theta}, \qquad (1)$$

where ω is the optical angular frequency, *c* the velocity of light, and *n* the refractive index chosen according to the beam polarization. In the absence of the external electric field, E_{sc} induced by the interference pattern is

$$E_{sc} = \frac{K_B T}{q}\frac{K\cos 2\theta}{1 + K^2/K_0^2} \qquad (2)$$

$$K = \frac{4\pi n}{\lambda}\sin\theta; \qquad K_0^2 = \frac{q^2 N_A}{K_B T \varepsilon\varepsilon_0}, \qquad (3)$$

where λ is the vacuum wavelength, $\varepsilon\varepsilon_0$ the dielectric constant along the grating vector, and 2θ the angle between the two beams. The γ_{eff} is the effective Pockel coefficient of the iron-doped potassium niobate crystal. For an extraordinary polarized beam γ_{eff} in c–b plane is[1]

$$\gamma_{\text{eff}} = \frac{\cos\beta}{2}[n_b^4\gamma_{23}(\cos 2\theta - \cos 2\beta) + 4n_b^2 n_c^2\gamma_{42}\sin^2\theta + n_c^4\gamma_{33} \cdot (\cos 2\theta + \cos 2\beta)], \qquad (4)$$

where r_{ij} are the elements of the linear electro-optic tensor, n_b and n_c the principal indices of refraction of wavelength λ. For potassium niobate crystals at λ = 514.5 nm, n_b = 2.395, n_c = 2.211, γ_{23} = 1.3 pm/V, γ_{33} = 64 pm/V, and γ_{42} = 380 pm/V.[2] The dependence of the exponential gain coefficient on angles β and θ according to Eqs. (1)–(4) is shown in Fig. 1.

It is found that the optimum value of β corresponding to the maximum Γ is approximately 40° to the *c* axis and is nearly independent of N_A over the range from 10^{16} cm^{-3} to 10^{17} cm^{-3}. An iron-doped potassium niobate crystal was cut as shown in Fig. 2. The grating vector is about 40° to the *c* axis in the c–b plane. The angle θ is chosen to be 8° for our

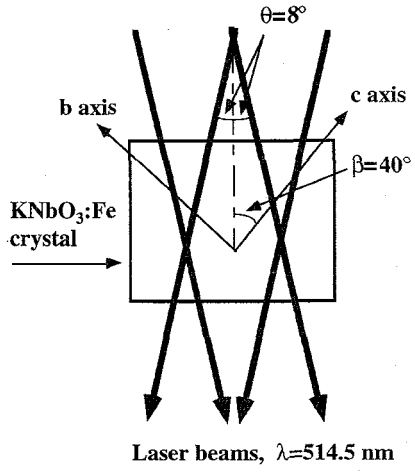

CTuP12 Fig. 2 Iron-doped potassium niobate crystal was cut as shown to reach the maximum photorefractive gain. Two writing laser beams are at λ = 514.5 nm with full angle 2β = 16°. The angle β is about 40°.

experiments. The special angle cut sample enables us to measure the hydrogen ions migration along both the *b* and *c* axes. It is found that the activation energies are 0.64 eV and 0.81 eV for hydrogen ion hopping along the *b* and *c* axes, respectively. A detailed process of thermal fixing in this sample is also discussed in the paper.

In conclusion, a special angle cut of iron-doped potassium niobate crystal was designed to achieve the maximum exponential gain coefficient for thermal fixing of volume holograms. A significant enhancement of diffraction efficiency of the fixed grating 43% is measured.

Hebrew University of Jerusalem, Jerusalem, Israel

1. Y. Fainman, E. Klancnik, S. H. Lee, Opt. Eng. **25,** 228 (1986).
2. P. Gunter, Phys. Rep. **93,** 199 (1982).

CTuP13

Photorefractive properties in Rh:$LiTaO_3$ in the ultraviolet and visible wavelength region

Y. Furukawa, K. Kitamura, Y. Ji, P. Bernasconi,* G. Montemezzani,* P. Günter,*
National Institute for Research in Inorganic Materials, 1-1 Namiki, Tsukuba, Japan 305

The development of materials with high nonlinearity, high sensitivity, and fast photorefractive effect is an important key to realization of a wide variety of optical processing applications. So far, large efforts have been performed in the development of several photorefractive crystals doped with different impurities. Iron-doped $LiNbO_3$ has recently attracted much attention for holographic memory applications because of its excellent photorefractive properties and its very long holographic storage times. Further, it can be produced in large sizes, thus being suitable for mass production. We have recently reported that a control of the nonstoichiometry defects in $LiNbO_3$ can improve the photorefractive properties.[1] We

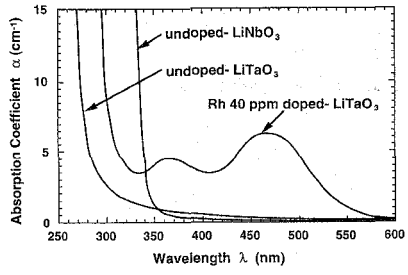

CTuP13 Fig. 1 Absorption spectrum of Rh-doped and undoped $LiTaO_3$ crystals.

have also successfully grown doped $LiTaO_3$ crystals that are known to have similar photorefractive properties as $LiNbO_3$.[2] Since commercially available undoped $LiTaO_3$ has a shorter absorption edge and shows less photorefractive optical damage than $LiNbO_3$, recent optical studies on $LiTaO_3$ have concentrated mainly on other nonlinear optical applications such as frequency conversion. However, it should be noted that by intentionally doping $LiTaO_3$ the photorefractive sensitivity can change by two orders of magnitude. In view of its transparency range extending till 280 nm suitably prepared and optimized $LiTaO_3$ crystals may hold much promise for any photorefractive applications at near ultraviolet wavelengths. The understanding and control of the photorefractive parameters of this crystal are therefore of great importance.

In this work, we show that Rh-doped $LiTaO_3$ has an enhanced two-beam coupling gain compared with undoped samples, both in the visible and ultraviolet wavelength region. We also investigate the influence of nonstoichiometricity on the photorefractive properties of $LiTaO_3$ and characterize the crystal samples in terms of the number of scattering centers that can serve as starting seeds for many self-pumped phase conjugation configurations.

Figure 1 shows the absorption spectra of undoped and doped $LiTaO_3$. Rh doping of 40 ppm introduces wide absorption near 375 and 472 nm, which is of great interest for photorefractivity in this short wavelength range.

Two-beam coupling measurements were performed at the wavelengths 532 and 363.8 nm with typical intensities of 10 W/cm^2 and 0.1 W/cm^2, respectively. Table 1 shows the two-wave mixing gain for several different kinds of crystals at 532 nm. Strong beam fanning was observed in both doped and undoped $LiTaO_3$ crystals, however high two-beam coupling exponential gain of 15 cm^{-1} was obtained only in the doped $LiTaO_3$ crystal. In the ultraviolet, an even larger exponential gain of 20 cm^{-1} has been observed in the Rh-doped samples.

Laser scattering centers inside the bulk of crystals samples has been characterized by a laser tomography system (MO-411, Mitsui Mining & Smelting Co. Ltd.).[3] This observation method allows one to obtain a sectional image of micro defects inside the bulk crystal in a nondestructive way. Figure 2a shows that Fe:$LiNbO_3$ contains some scattering centers. However, by a careful control of the crystal growth conditions,[1] the number of scatterers